A fully automatic polygon scaled boundary finite element method for modelling crack propagation

Shangqiu Dai[a,*]; Charles Augarde[b]; Chengbin Du[a]; Denghong Chen[c]

[a] Department of Engineering Mechanics, Hohai University, Nanjing 210098, China

[b] School of Engineering and Computing Sciences, Durham University, Durham DH1 3LE, UK

[c] College of Civil Engineering and Architecture, China Three Gorges University, Yichang 443002, China

Abstract:

An automatic crack propagation remeshing procedure using the polygon scaled boundary FEM is presented. The remeshing algorithm, developed to model any arbitrary shape, is simple yet flexible because only minimal changes are made to the global mesh in each step. Fewer polygon elements are used to predict the final crack path with the algorithm as compared to previous approaches. Two simple polygon optimisation methods which enable the remeshing procedure to model crack propagation more stably are implemented. Four crack propagation benchmarks are modelled to validate the developed method and demonstrate its salient features.

Keywords:

Scaled boundary finite element method; Crack propagation; Fracture; Polygon elements

1. Introduction

Fracture in brittle materials is an important issue in structural damage and failure. Modelling mixed-mode crack propagation in this material, combined with linear elastic fracture mechanics (LEFM), is an active research field and considerable efforts have been made in recent years. Studies are usually implemented within four broad frameworks, i.e. the finite element method (FEM), the boundary element method (BEM) and two more recent numerical approaches: meshless methods and extended FE methods.

[*]Corresponding author at: Department of Engineering Mechanics, Hohai University, Nanjing 210098, China.
Tel: +07821 287206.
E-mail address: hhudsq@gmail.com

Nomenclature

B^1, B^2	Linear operator matrices of the SBFEM system
c	Integration constants of the SBFEM system
D	Elasticity matrix
E^0, E^1, E^2	Coefficient matrices of the SBFEM system
K	Global stiffness matrix
K_{si}	Stiffness matrix of one subdomain
$K_{\mathrm{I}}, K_{\mathrm{II}}$	Model-I and model-II stress intensity factors
L_0	Distance between the crack tip and the boundary
N	Shape function
P	Equivalent nodal force
P_{si}	Equivalent nodal force of one subdomain
u	Displacement field
Δa	Crack increment length
ξ, s	Local coordinate system of the SBFEM system
r, θ	Polar coordinates
λ	Diagonal matrix
φ	Displacement vector of the SBFEM system

Since the FEM was first used to model crack propagation in reinforced concrete beams by Ngo and Scordelis [1], it has been the predominant numerical method for crack problems [2-4]. However, crack propagation modelling with the FEM is still a challenging subject, because it usually requires both fine crack tip meshes [5-6] and sophisticated remeshing algorithms during crack propagation [7-8] to accurately calculate fracture parameters such as stress intensity factors (SIFs). Various methods have been proposed to extend the application of the FEM, such as the superposition method [9], quarter-point elements [10], and hybrid crack elements [11]. The extended FEM (XFEM) [12] and meshless methods [13] using nodal enrichment techniques, which can model crack propagation without remeshing, have been proposed more recently as alternatives to tackle the difficulties faced by the FEM in crack propagation modelling. Serious crack propagation problems both in statics and dynamics have been solved with these two methods [14-17]. However, fine meshes (in the case of XFEM) and fine nodal distributions (in the case of meshless methods), are still needed, especially when the crack paths are unknown in advance [18].

The BEM is a competitive alternative to FEM in crack propagation modelling because only the boundaries of the problem domain are discretised to define the geometry and only new boundary elements need to be added to the crack tip during remeshing. Although the BEM has these appealing features, its requirement of fundamental solutions limits its applicability considerably, generally to linear problems. Enormous research effort has sought to improve the existing BEM approach, with

new techniques evolving such as the dual boundary element method (DBEM) [19] and the dual reciprocity method [20], but more exciting progress seems likely with enriched BEM methods [21].

The scaled boundary finite element method (SBFEM), is a semi-analytical method and was first developed by Wolf and Song [22] in the 1990s. It not only combines the advantages of FEM and BEM, but also possesses key features to make crack modelling more effective and efficient, and also has useful attributes such as the ease with which accurate SIFs can be extracted directly from the semi-analytical solutions [23-24] without fine crack tip meshes or special elements. Due to these attributes, the SBFEM has been successfully coupled with the BEM [25] and XFEM [26-27] for calculating parameters in fracture mechanics. These advantages have also been exploited in modelling both static and dynamic crack propagation problems by developing a simple remeshing procedure based on LEFM [18, 28]. The advantage of the remeshing procedure is more significant when combined with cohesive interface finite elements (CIEs), a method named the FEM-SBFEM coupled method [29-31], to model cracks in nonlinear fracture mechanics (NFM). However, for problems with arbitrary multiple cracks in any arbitrary domain, the remeshing method is a little cumbersome because the subdomains may become so distorted that not all the nodes are directly visible from the scaling centres (an issue discussed in detail later in this paper).

A more general implementation of the SBFEM, where subdomains are discretised with polygon elements, was proposed by Ooi et al. [32-33] to overcome the problems described above. Polygon elements permit meshing of complex geometries flexibly, and the method uses a very simple local remeshing algorithm which just makes minimal changes to the global mesh by modelling the crack from one subdomain into an adjacent subdomain. However, the polygon mesh has to be refined in order to calculate the crack path accurately, because the crack propagation length is determined by the average distance from the vertices of the cracked subdomain to its scaling centre. Although a robust remeshing technique [34-35] was later proposed by Song and colleagues, similar to the hybrid FEM-SBFEM [36-37], the background mesh in this method needs to be stored and updated throughout the entire simulation, which makes it potentially computationally inefficient.

Recently, the polygon SBFEM was proved to be more accurate when compared with the conventional polygon FEM and cell-based smoothed polygon FEM [38] and a scaled boundary polygon formulation was developed to model elasto-plastic material responses in structures [39], which increases the application possibilities of the polygon SBFEM.

This study extends the simple remeshing algorithm developed in [18, 28] to model polygon scaled boundary elements in brittle materials with any arbitrary shape. This remeshing algorithm is augmented to enable the modelling of crack propagation more stably and accurately. This paper is organized as follows: Section 2 briefly discusses the polygon SBFEM and its procedures for computation of SIFs. Section 3 discusses the pre-processing module used to generate polygon elements based on open-source Delaunay tessellation software. Section 4 addresses the remeshing algorithm and its improvement applied to the polygon SBFEM. Section 5 demonstrates the application

of the algorithm to three mixed-mode crack propagation examples and section 6 summarises the major conclusions that can be drawn from this study.

2. Polygon scaled boundary finite element method

The basic concept of the SBFEM is illustrated in Figs1a and 1b. Fig.1a shows a typical domain of arbitrary shape modelled by four subdomains, in which subdomain 1 contains a crack (named the cracked subdomain). Each subdomain has a scaling centre, from which all the boundaries of this subdomain are visible. Only the boundaries of the subdomains are discretized, by three-node line elements as shown in Fig.1a. Fig.1b shows the details of the cracked subdomain. In the cracked subdomain, the scaling centre is positioned at the crack tip and two side-faces (named crack edges) which are connected to the scaling centre are not discretised. The coordinates of the nodes on the boundaries are uniquely defined by a local coordinate system (ξ, s) whose origin is at the scaling centre. One circumferentially similar curve with $\xi = 0.5$ is also shown in Fig.1b.

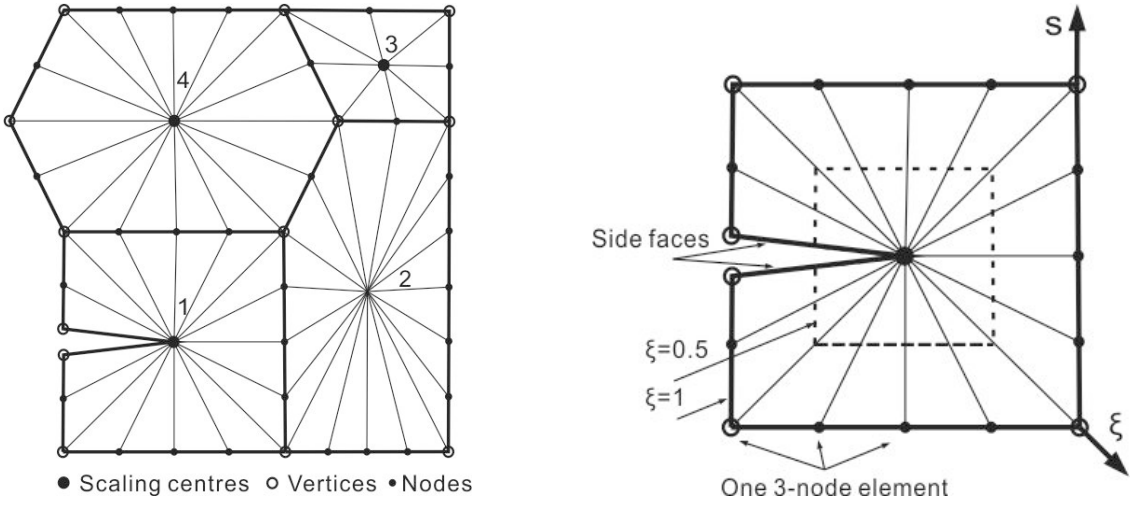

(a) SBFEM subdomains (b) The crack subdomain

Fig.1 The concept of the scaled boundary finite element method

The key governing equilibrium equations of SBFEM for elastostatics can be derived as in [40] using the virtual work principle:

$$P = E^0 u(\xi)_{,\xi} + E^{1^T} u(\xi)|_{\xi=1} \tag{1}$$

$$E^0 \xi^2 u(\xi)_{,\xi\xi} + \left(E^0 + E^{1^T} - E^1\right)\xi u(\xi)_{,\xi} - E^2 u(\xi) = 0 \tag{2}$$

where P is the equivalent nodal force vector due to the boundary tractions, and E^0, E^1, and E^2 are coefficient matrices that depend on the geometry and material properties of the subdomain. $u(\xi)$ represents the nodal displacements and comprises N analytical functions of the radial coordinate ξ where N equals the total number of degrees of freedom (DOFs). By inspection, the solution $u(\xi)$ of Eq. (2) for each subdomain must be of the following form:

$$u(\xi) = \sum_{i=1}^{N} c_i \xi^{\lambda_i} \varphi_i \tag{3}$$

where the exponents λ_i and corresponding vectors φ_i are N positive eigenvalues (which can be identified as a modal scaling factor in the ξ direction) and eigenvectors (which can be identified as the modal displacements at the boundary nodes) of a standard eigenproblem. The eigenvalues and eigenvectors depend on the boundary geometry, material properties and nodal discretization scheme of the subdomain. The N modal displacements are designated by $\Phi = \{\varphi_1, \varphi_2, \dots, \varphi_N\}$. The integration constants c_i represent the contribution of each mode to the solution and are dependent on the boundary conditions [40].

The global stiffness matrix and load vector can be obtained by assembling the stiffness matrix of all the subdomains in a manner similar to FEM, i.e.

$$K = \sum_{i=1}^{N_s} K_{si} \text{ and } P = \sum_{i=1}^{N_s} P_{si} \tag{4}$$

where $\mathrm{N_s}$ is the number of subdomains and $\mathrm{K_{si}}$ can be obtained as:

$$\mathrm{K_{si}} = \mathrm{E^0}\Phi[\lambda]\Phi^{-1} + \mathrm{E^{1^T}} \tag{5}$$

where the diagonal matrix $[\lambda] = diag(\lambda_1, \lambda_2, \dots, \lambda_N)$.The global nodal displacements on the whole boundary can be obtained from the equilibrium equation after considering the displacement constraints and external loading conditions, from

$$Ku_b = P \tag{6}$$

The integration constants c_i required to satisfy Eq. (3) on the boundary are

$$\mathrm{c} = \Phi^{-1}\mathrm{u_{bs}} \tag{7}$$

where $\mathrm{u_{bs}}$ is the nodal displacements on the boundary of one subdomain and is one subset of $\mathrm{u_b}$.
The displacement field of each subdomain then can be recovered by

$$u(\xi, s) = N(s)\left[\sum_{i=1}^{N} c_i \xi^{\lambda_i} \varphi_i\right] \tag{8}$$

where $\mathrm{N(s)}$ is the shape functions in the circumferential direction, which are constructed as in the FEM.

The stress field in the subdomain can be obtained by

$$\sigma(\xi, s) = D\sum_{i=1}^{N} c_i \xi^{\lambda_i - 1}[\lambda_i B^1(s) + B^2(s)]\varphi_i = \begin{Bmatrix}\sigma_{xx}\\ \sigma_{yy}\\ \sigma_{xy}\end{Bmatrix} \tag{9}$$

where D is the elasticity matrix and $B^1(s)$ and $B^2(s)$ are matrices which depend on geometry of the subdomain [40].

Fig. 2 shows a cracked domain modelled by the SBFEM. Based on the Williams eigenfunction expansion around the crack tip [24], accurate SIFs can be directly extracted from the semi-analytical solution (Eq. (9)) when both the origin of a Cartesian coordinate system is at the crack tip and the x-axis is along the line of the crack. The SIFs are then as follows:

$$\begin{Bmatrix}K_{\mathrm{I}}\\ K_{\mathrm{II}}\end{Bmatrix} = \begin{Bmatrix}\sum_{i=1,2}\sqrt{2\pi L(\theta)}c_i\sigma_{yy}(s)_i|_{\theta=0}\\ \sum_{i=1,2}\sqrt{2\pi L(\theta)}c_i\sigma_{xy}(s)_i|_{\theta=0}\end{Bmatrix} = \sqrt{2\pi L_0}\sum_{i=1,2}\left(c_i\begin{Bmatrix}\sigma_{yy}(s_A)\\ \sigma_{xy}(s_A)\end{Bmatrix}\right) \tag{10}$$

where $L_0 = L(\theta = 0)$ is the distance between the crack tip and the point A at the crack edge direction on the boundary (shown in Fig.2) and $i = 1,2$ represents the two modes each corresponding to $\lambda = 0.5$ which leads to the square-root singularity according to [24].

When a crack edge is at an arbitrary direction during the crack propagation, the stress in Eq. (11) should first be transformed into normal stress σ_n and shear stress τ_n on the crack surface plane at point

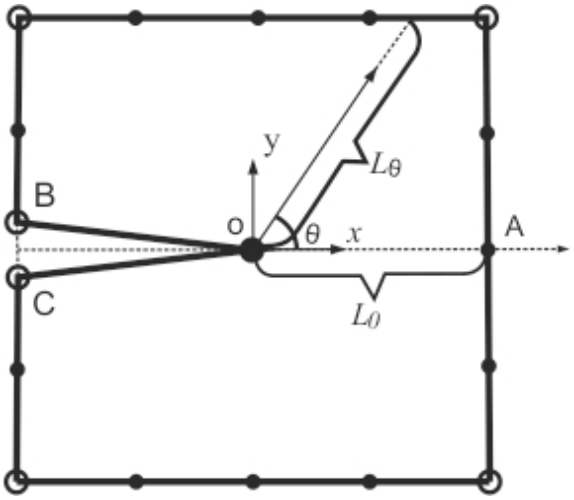

Fig. 2 A crack subdomain modelled by SBFEM

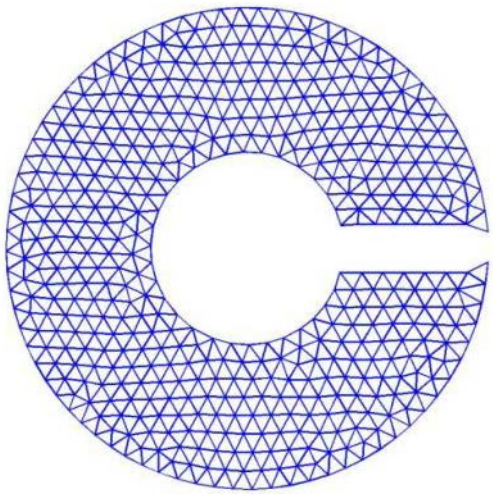

Fig. 3 A triangulated mesh

A separately.

$$\begin{Bmatrix} K_{\mathrm{I}} \\ K_{\mathrm{II}} \end{Bmatrix} = \sqrt{2\pi L_0} \sum_{i=1,2} \left(c_i \begin{Bmatrix} \sigma_n(s_A) \\ \tau_n(s_A) \end{Bmatrix} \right) \tag{11}$$

It should be noted that the stresses at point A can be directly obtained by Eq. (9), so the point A does not need to be an existing node.

3. Generation of polygon scaled boundary finite elements

The open-source Delaunay tessellation, named Distmesh, is a Matlab program which can generate a triangulated mesh for a variety of geometric domains. It is a relatively simple and flexible program which requires only two basic functions fd and fh to control the meshing, which represent the distance function defining the domain and a mesh density function controlling the element density respectively. Fig. 3 shows a triangulated mesh generated by the program with the shape of 'Big C' [41]. N-sided polygon elements then can be generated by a simple procedure from the triangulation.

The procedure proposed in this study is based on [32], but fewer nodes are used to generate the boundary polygon element (the element which contains the boundary edge) compared with the former method. To illustrate this more clearly, a simple rectangular domain is shown in Fig. 4 where the nodes of the triangles are divided into three groups: the interior nodes (within the domain), the exterior nodes (on the boundary) and the inflection nodes (reflecting the shape of the domain). Both the midpoints on the edges of the triangular elements on the boundary and the centroids of all the triangular elements are computed firstly.

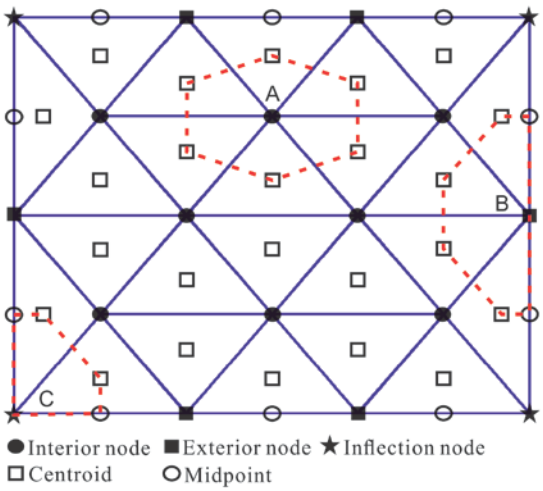

Fig. 4 Generation of the scaled boundary polygon finite elements

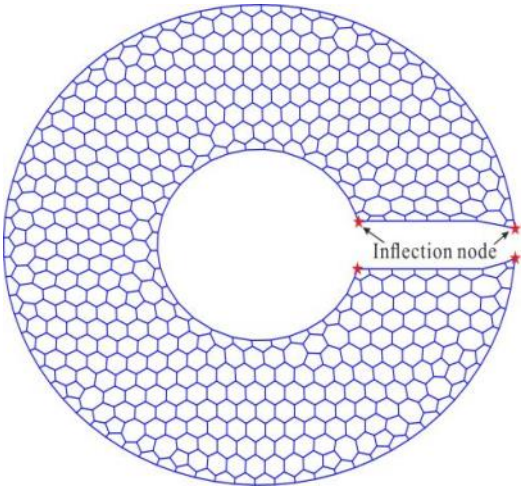

Fig. 5 The polygon element mesh of the 'Big C'

According to the three different types of the triangular nodes, the polygon elements can be generated in the following three ways. For a typical interior node A of the triangular mesh, a 6-sided polygon element (interior polygon element) can be generated by connecting the centroids of all the triangular elements immediately surrounding node A, and node A is defined as the scaling centre of this element. For a typical exterior node B, the two midpoints of the boundary edges connecting to it and four centroids of the triangles around it are used to construct the boundary polygon element. The scaling centre of the element depends on the coordinates of the six points around node B. For a typical inflection node C, because the boundary polygon element should also represent the shape of the domain accurately, the inflection node is added to define the polygon element. In Fig. 4 for example, the three typical polygon elements are plotted in red. Compared with the procedure in [32], only relatively few boundary polygon elements contain the inflexion nodes, so the total number of degrees of freedom is reduced as compared to the previous procedure. This can be significant when the mesh is fine or the domain contains a long boundary.

The domain can then be discretised into polygon elements according to the procedures outlined above. Fig 5 shows a polygon SBFEM mesh based on the triangular mesh denoted 'Big C', which only has four inflection nodes. It can be seen that the mesh is regular and all the polygons are convex. In the later computations presented here, each polygon element is regarded as one subdomain and its vertices are arranged in an anticlockwise direction. Combining with load and crack information, the polygon element mesh can be directly used for the calculation.

4. Remeshing with the polygon scaled boundary finite element method

4.1 Local remeshing

The remeshing algorithm developed in [18, 28] is very efficient for problems with a single crack, or a few cracks that are far away from each other in a simply shaped domain. Its extension to crack propagation problems in arbitrary domains, however, can be cumbersome because the subdomains

may become so distorted that not all the nodes are visible from the scaling centres, a fundamental problem with the SBFEM. In this study, this remeshing algorithm is augmented to accommodate crack propagation of arbitrary shapes based on the use of polygon element meshes.

The procedure is as follows. The location of the new crack tip in each crack propagation step should be first determined, based on both the specified crack propagation length Δa (which is usually user-defined in simple incremental analysis) and the crack propagation direction θ_c. Once the SIFs have been calculated from Eq. (11), three common theories can be used to compute θ_c: (1) the maximum circumferential stress theory (σ_{max}criterion); (2) the maximum energy release rate theory (G_{max}criterion); and (3) the minimum strain energy density theory (S_{max}criterion) [28]. At any crack propagation step, the remeshing algorithm can be divided into four cases according to the crack tip's location: (1) a crack first propagates in one subdomain; (2) a crack goes on propagating in one subdomain; (3) a crack propagates into another subdomain; and (4) the crack propagates outside the domain which leads to the end of the propagation.

The remeshing procedure for case 1 is outlined in Fig. 6 for one crack propagation step. Given Δa and θ_c, the location of the new crack tip, shown in Fig. 6(a), is calculated and located in the cracked subdomain (point A is used to computer the SIFs). The former crack tip is then separated into two new vertices ($V_1$and V_2 in Fig. 6(b)). Two new subdomains (1 and 2) are generated along with four new edges ($E_1$to E_4). The new edges and subdomains are only used to record the crack path and guarantee all the edges of the new cracked subdomain (3) are visible from the new crack tip. There is no need to generate the so-called 'core subdomains' required in the previous methods [18, 28] before the beginning of the crack propagation.

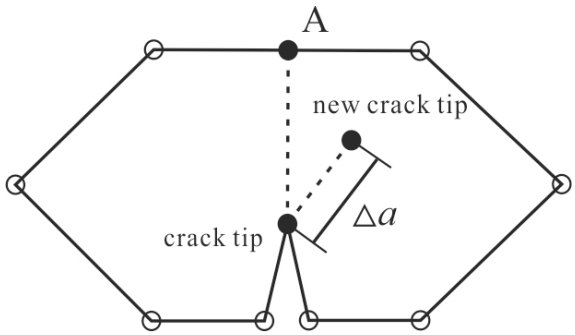

Fig. 6(a) New crack tip for Case 1

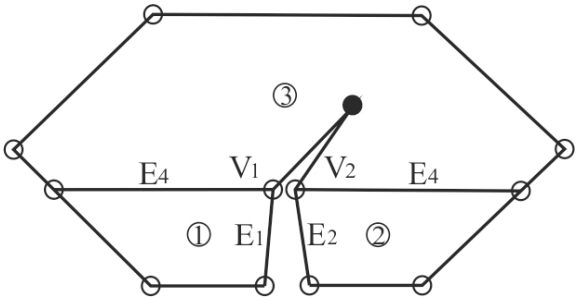

Fig. 6(b) Final mesh in Case 1

Fig. 6 The remeshing procedure for case 1

The remeshing procedure for case 2 is outlined in Fig. 7 for one crack propagation step. When Δa is smaller than the subdomain's size, the crack will propagate in the same subdomain after the first propagation step (Fig. 8(a)). Since the geometry of a polygon element can be complex, the new scaling centres which are automatically generated may not be seen easily from all the edges of the new subdomains. Therefore the shapes of subdomains 1 and 2 must be checked for the convex segment firstly to guarantee the necessary requirement of SBFEM. The remeshing procedure is very simple

when the shapes are both convex, following the procedure in [18, 28], just enlarging the two subdomains (1 and 2) by adding four new vertices ($V_5$to V_8) and moving the two former edges ($E_1$and E_2) to $E_3$and E_4, as shown in Fig. 8(b). To complete the remeshing, the convex segment is applied again before generating the new scaling centres. The scaling centre of subdomain 2, which is still convex, is moved to the new geometric centre (centroid) and the new crack tip becomes the scaling centre of subdomain 3. As to subdomain 1 which is now concave, the new scaling centre is chosen as the centre of the shadow domain automatically as shown in Fig. 7(c), in which points A and B are intersection points between the crack path and the edges of subdomains. If either of the subdomains is concave, like subdomain 1 in Fig. 7(b), the subdomain maintains its shape to avoid over-distortion during the next propagation steps, and a new subdomain is generated to represent the new crack path at this step. At the same time, another convex subdomain can be remeshed using the former method. This leads to the final mesh shown in Fig. 7(d), in which subdomain 4 is the new subdomain. In the next step, subdomain 4 is used to check for the convex segment instead of subdomain 1. This procedure generates the new scaling centres automatically and guarantees that all the edges of the new polygons after remeshing are visible from their scaling centres and each subdomain has one concave point at most.

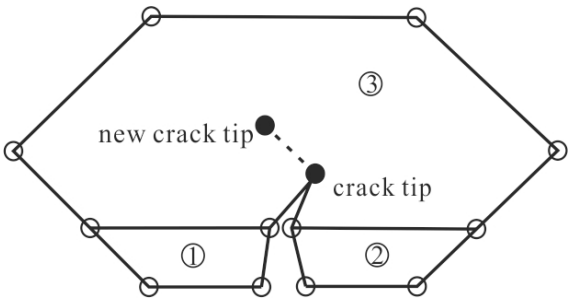

(a) New crack tip for Case 2

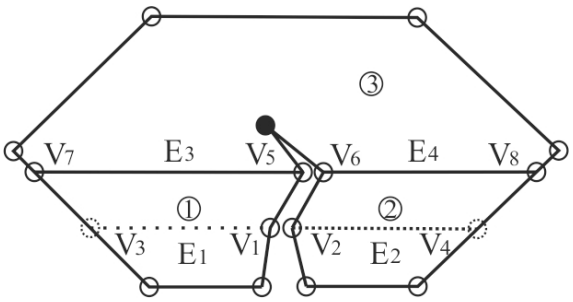

(b) Final mesh in Case 2 (one step)

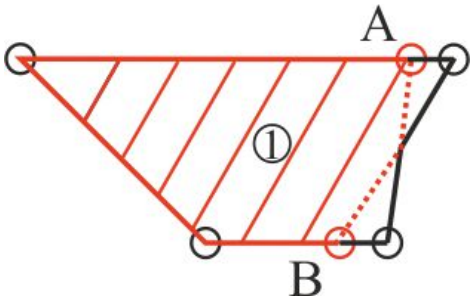

(c) The shadow domain in subdomain 1

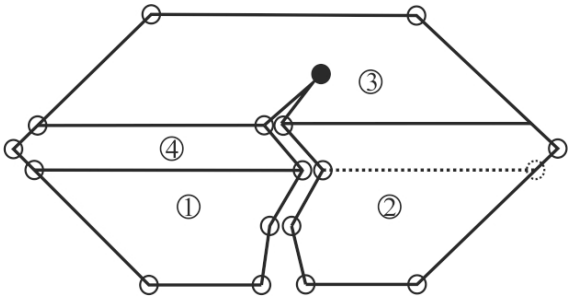

(d) Final mesh in Case 2 (two steps)

Fig. 7 The remeshing procedure for case 2

When the new crack propagates into another subdomain, it becomes case 3. Point B in Fig. 8(a) is the intersection point between the crack path and the edge of subdomains. Fig. 8(b) shows the remeshing procedure. First, both the former crack tip and point B are separated into two vertices (V_1-V_2 and V_3 - V_4). Next, four new edges ($E_1$to E_4) are added to the cracked subdomain (2), which are used to record the crack path. As a result, the cracked subdomain is split into two normal subdomains

(2 and 3). After checking whether the two subdomains are convex or concave, the scaling centres of the two subdomains are placed at their geometric centres or the shadow domain's centres separately. Subdomain 1 now turns into the new cracked subdomain with the two side-faces E_5 and E_6, and resembles the cracked subdomain shown in Fig. 6(a). Therefore, the situation reverts to case 1 after this crack propagation step.

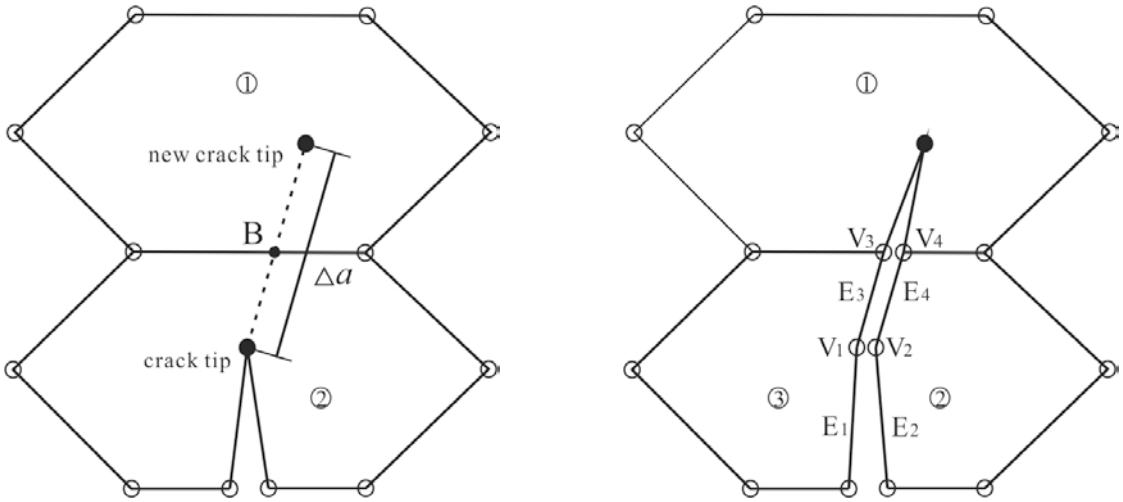

(a) New crack tip for Case 3 (b) Final mesh in Case 3

Fig. 8 The remeshing procedure for case 3

The remeshing procedure for case 4 is outlined in Fig. 9 for one crack propagation step. It resembles the procedure in case 3 outlined in Fig. 8. The differences between them are the crack path only extends to the intersection point on the boundary and this step leads to the end of the procedure. In Fig. 9(b), for example, point B is the intersection point and is not separated.

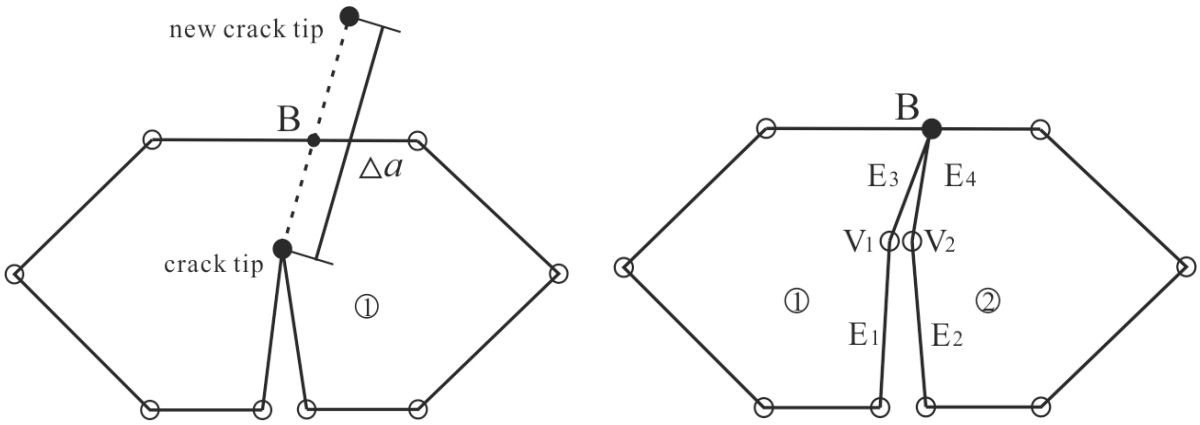

(a) New crack tip for Case 4 (b) Final mesh in Case 4

Fig. 9 The remeshing procedure for case 4

It is worth noting that this algorithm only minimally alters the global mesh structure in all four cases, confining refinement to a very small region of the domain. Only the cracked subdomain and the adjacent subdomains are used during each crack propagation step. Compared to the procedure

previously devised in [18, 28], the new subdomains are only used to record the crack path and the convex segment makes sure the procedure is more stable as modelled using polygon elements.

4.2 Polygon optimisation

When the simple remeshing procedure is applied to the polygon SBFEM, the procedures to arrive at the convex segment can in some cases be insufficient to guarantee high accuracy during calculation. The reason for this is that it can lead to a cracked polygon in which the new crack tip is placed very close to one polygon edge or vertex, as shown in Fig. 10(a) and (b). This is undesirable from a numerical point of view and can lead to errors in the computed displacements and SIFs. Here we take account of this possibility by including a further shape optimisation step via two methods.

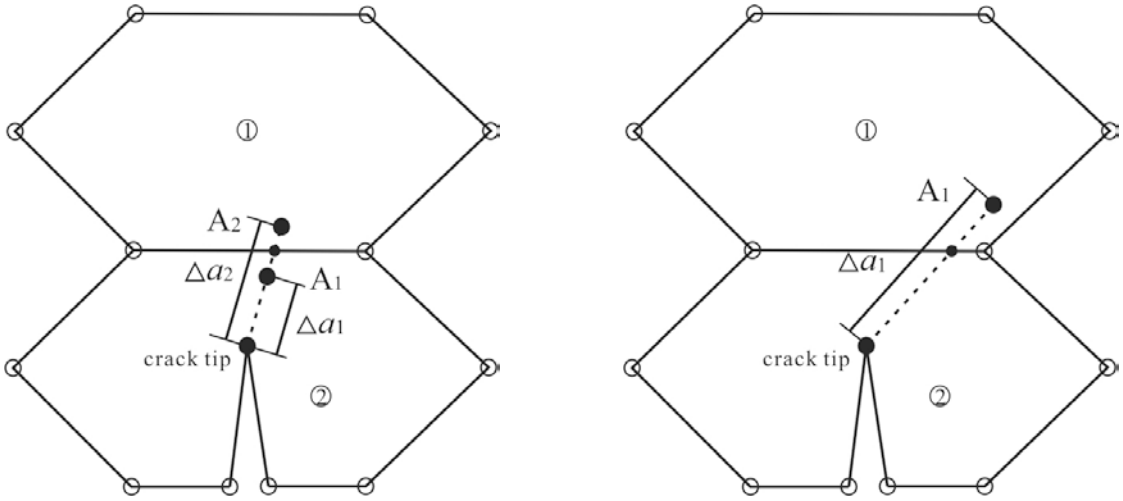

(a) Situation 1 (b) Situation 2

Fig. 10 Polygon optimisation for new crack tips that are too close to a polygon edge or vertex

Due to the value of Δa, the new crack tip may located at A_1 or A_2 shown in Fig. 10(a), which is very close to one edge. For this situation, the half-length of $\Delta a1$ and double-length of $\Delta a2$ can be adopted as an alternative Δa to recalculate the new crack tip's location. A second approach to use when the intersection point is too close to either of the vertices is shown in Fig. 10(b), where a simple polygon optimisation method is proposed by reconstructing three adjacent subdomains. In Fig. 11, for example, after the remeshing procedure, vertex B is dragged to point C which makes the new edge's length 1.5 times as long as originally. Then, two new edges $E_3$and E_4 instead of $E_1$and E_2 are used to regenerate the three subdomains (1 to 3). Lastly, after checking whether they are convex or concave, the scaling centres of subdomain 2 and 3 are generated automatically according to the former method. It can be seen that the cracked subdomain (1) now has a better shape. Sometimes the new crack tip may be too close to the edge and vertex at the same time. The two methods then should be applied to the cracked subdomain together.

4.3 Numerical implementation

Fig. 12 shows a simplified flow chart of the remeshing algorithm for crack propagation. The pre-processing unit generates the polygon SBFEM mesh and inputs it with the load and crack information into the analysis unit. The analysis unit then computes the nodal forces and displacements which are used to calculate the SIFs and θ_c. After the solution is obtained from the analysis, one of the three theories can be used to check whether the crack propagates or not. If the propagation condition is satisfied, a new location of the crack tip is calculated. The remeshing procedure, which embodies the major portion of the study reported herein, is shown clearly in Fig. 12. The location of the new crack tip is first checked to see whether the shape of the cracked subdomain is acceptable. If the location is not suitable, the two methods, i.e. modifying Δa and/or reconstructing the adjacent subdomains' shape, are applied until the shape is acceptable. Next, the remeshing procedure is carried out according to the four different cases. After one propagation step, if it is not a case 4 situation, the procedure then proceeds to analysis unit again leading to the next propagation step.

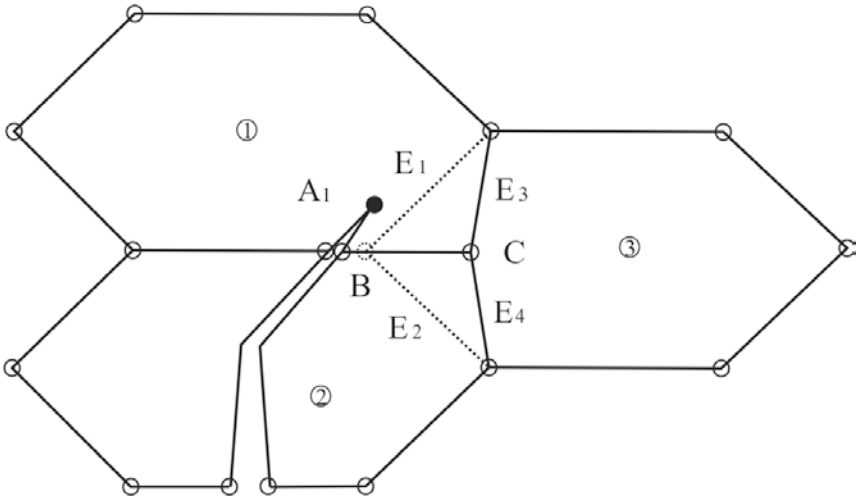

Fig. 11 Final mesh after polygon optimisation method

5. Numerical examples

In this section four fracture problems are modelled using the remeshing algorithm presented above. Each edge of elements in the three problems is discretised using two 3-node elements.

The first example is a PMMA edge-cracked plate which was modelled by Swenson and Kaushik [42] and Yang [28] separately. Fig. 13(a) shows the geometry, boundary and loading conditions and material properties of the specimen, in which the length unit is mm. A coarse and a fine polygon mesh (Fig. 13(b) and (c)) with 73 and 265 polygons respectively are used to calculate the crack path with an initial crack position $d = 10mm$. According to the different sizes of the polygons, the crack propagation length chosen for the coarse mesh $\Delta a = 2.5mm$ and for the fine mesh $\Delta a = 1.5mm$. A plane strain condition and σ_{max}criterion are assumed in this example.

Fig. 14(a) and (b) show the predicted crack paths of the two meshes, in which the asterisk represents the crack tip position in each propagation step. In order to guarantee the accuracy of the computed displacements and SIFs, the polygon optimisation method is automatically applied during the propagation which changes the shapes of some polygon elements on the crack path (the red polygons shown in Fig. 14). It can be seen that the crack paths obtained from both the meshes are similar. As the load is applied, the crack initially propagates in approximately a straight line and then curves toward the free surface as it approaches the bottom boundary. These features are captured by both coarse and fine meshes and are in good correspondence with the results of FEM [42] and SBFEM [28] as shown in Fig. 15. It is also evident in Fig. 15 that the predicted crack paths are not sensitive to the mesh used and the coarse mesh delivers high accuracy of the crack path based on the significant feature of SBFEM.

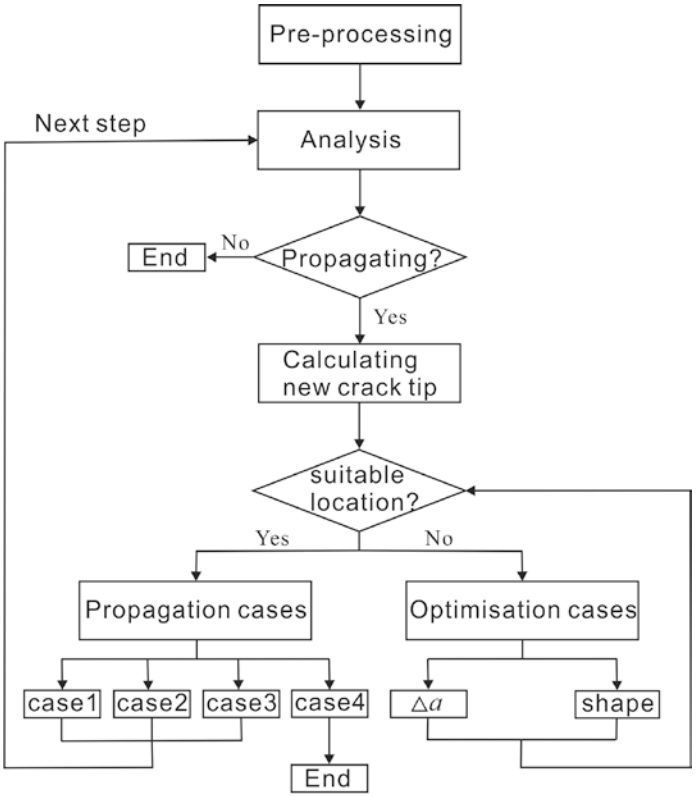

Fig. 12 Flow chart of the remeshing algorithm for crack propagation

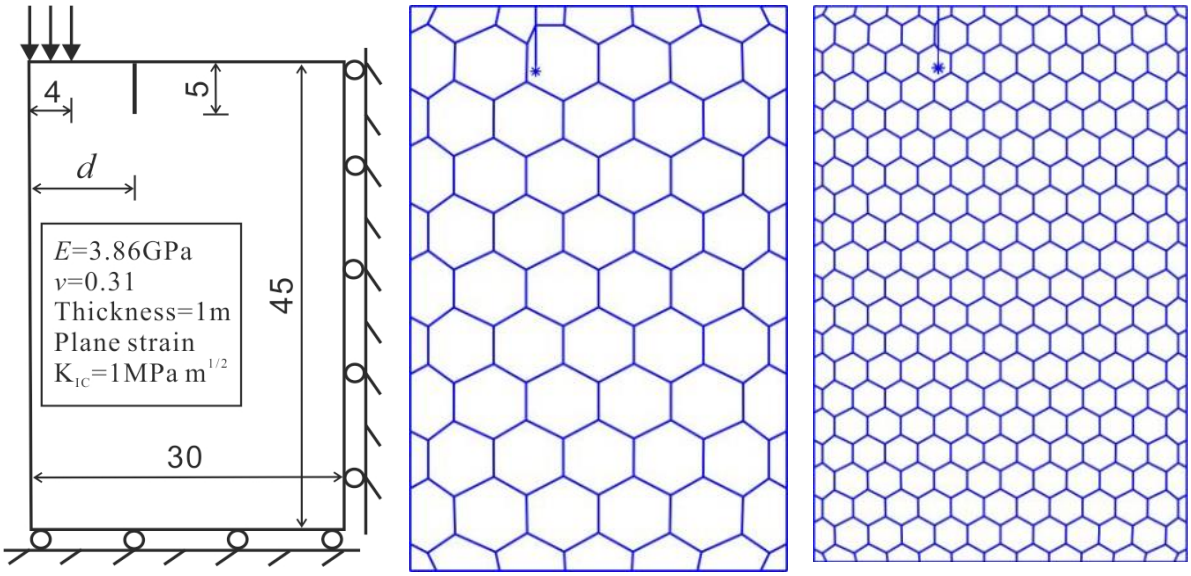

(a) The geometry (b) The coarse mesh (c) The fine mesh

Fig. 13 A PMMA edge-cracked plate

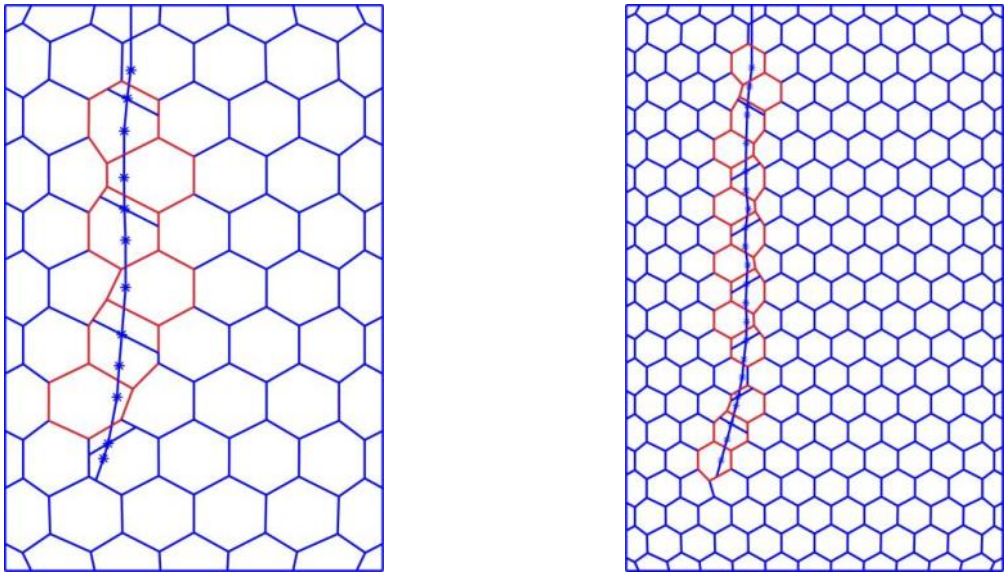

(a) The coarse mesh (b) The fine mesh

Fig. 14 Predicted crack propagation paths in a PMMA edge-cracked plate

The coarse mesh then used to examine crack curvature for cases in which the initial notch is positioned to the left ($d = 6mm$) or right ($d = 14mm$) of the crack location in Fig. 14. Results for these calculations are superimposed and shown in Fig. 16. As can be seen, they all converge to the same location which agrees well with the simulation results in [42].

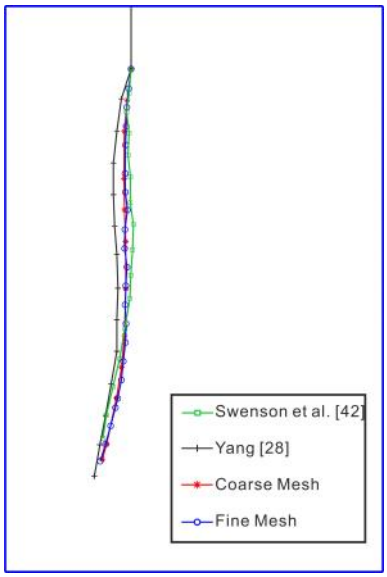

Fig. 15 Comparison of crack paths

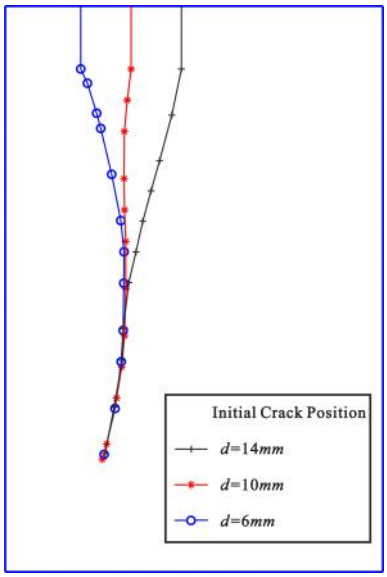

Fig. 16 Final paths for variation in d

The second example is a four-point single-edge notched shear concrete beam, which has become a benchmark for validating LEFM-based and NFM-based mixed-mode crack propagation models [28]. The geometry, boundary and loading conditions and material properties of the specimen are shown in Fig. 17(a). A plane stress condition is assumed in this example. Three crack increment length $\Delta a = 30mm, 35mm$ and $40mm$ are simulated using the same initial mesh shown in Fig. 17(b). The number of polygon elements is 58.

Fig. 17(c) shows the predicted crack propagation path in the beam with $\Delta a = 30mm$. During loading, the crack curves from its initially almost horizontal position, and then reorients itself almost vertically towards the top edge of the beam. Fig. 17(d) compares the crack paths predicted with the three crack increments and the result obtained by the simulation of Yang [28]. As can be seen from the figure, the crack paths are close to Yang's simulation and stable with different crack increments.

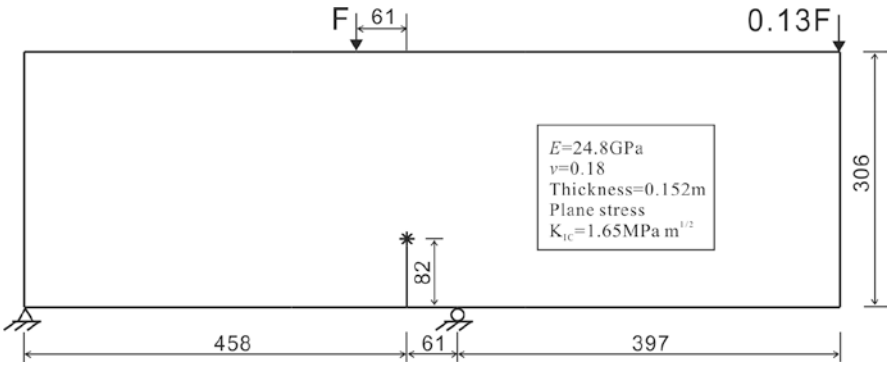

(a) Geometry

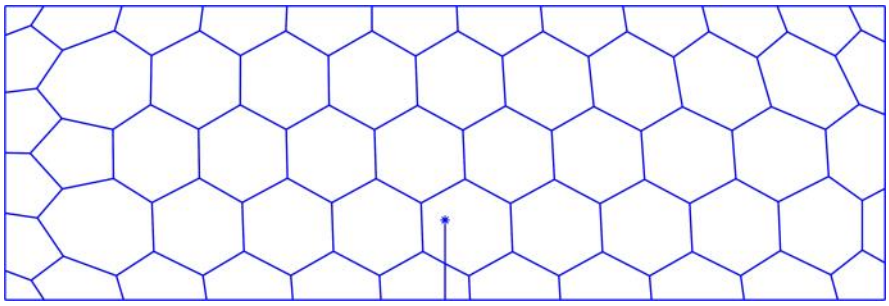

(b) SBFEM mesh with 58 polygon elements

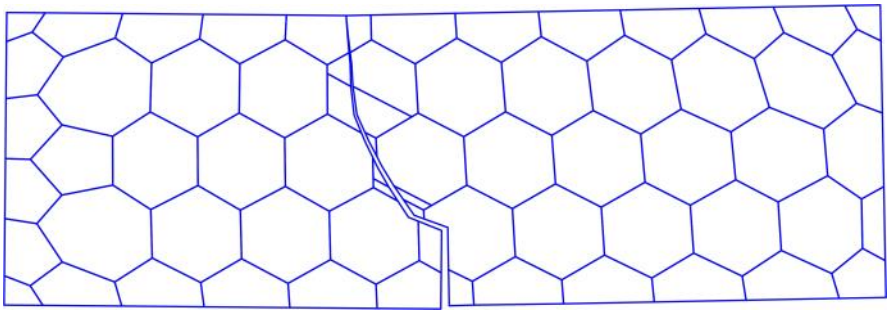

(c) Predicted final crack path

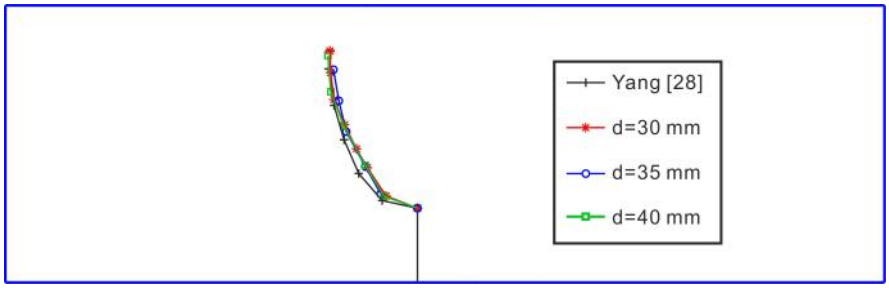

(d) Comparison of predicted crack paths

Fig. 17 Predicted final crack paths of a four-point single-edge notched beam

The third example is an edge cracked plate containing an off-centre circular hole shown in Fig. 18(a). The plate is loaded by uniform normal traction along the top and bottom edges. The material is assumed to be purely elastic with Young's modulus, $E = 98$ GPa and Poisson's ratio, $\nu = 0.3$ and the value of $K_{IC} = 1000\text{N/mm}^{3/2}$ as in [32]. Plane stress conditions are assumed in this example. This example was modelled by Rashid [43] using the arbitrary local mesh replacement method, Bouchard [44] using a local remeshing technique and Ooi et al. [32] using polygon SBFEM method. Compared with [32] which contain 497 polygon elements, a SBFEM mesh with 193 polygon elements is shown in Fig. 18(b).

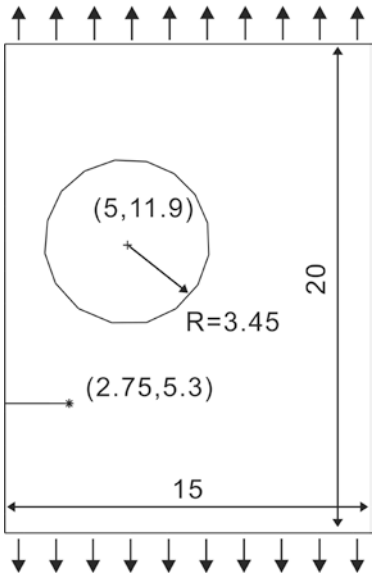

(a) Geometry(all dimensions in mm)

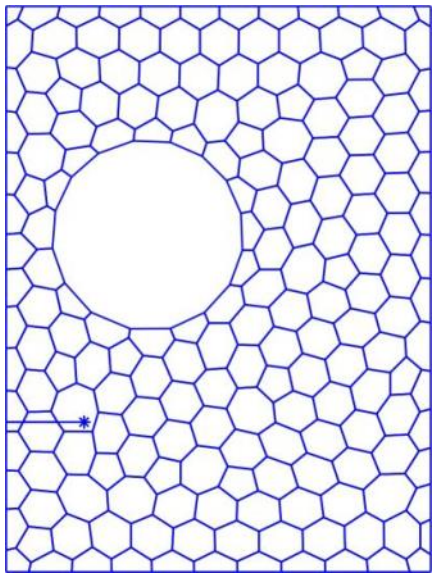

(b) The polygon SBFEM mesh

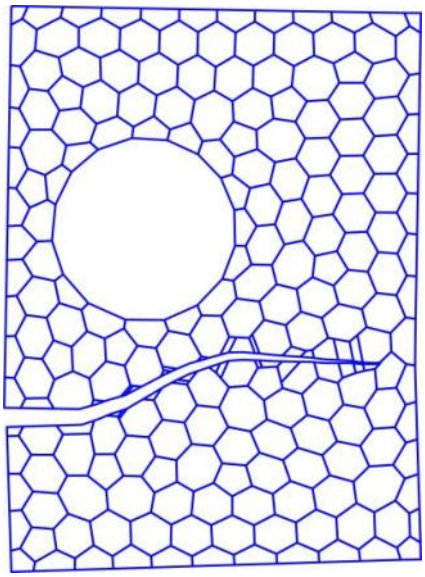

(c) Predicted final crack path

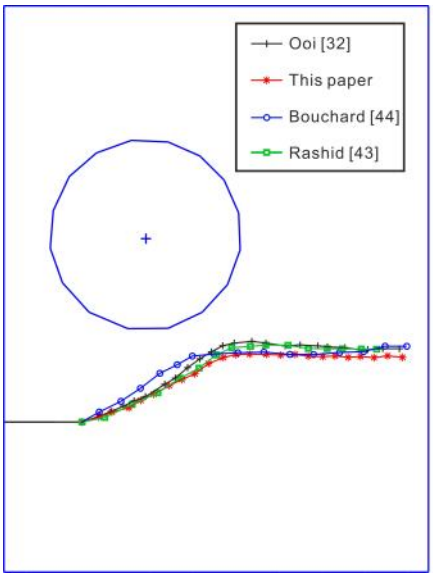

(d) Comparison of crack paths

Fig. 18 Predicted final crack paths of the plate with a hole

Fig. 18(c) shows the predicted crack path with the crack increment length $\Delta a = 0.5mm$. During loading, the crack firstly curves towards the hole because of the stress concentration within the vicinity of the cavity. After that, the crack reorients itself and propagates almost horizontally to the right edge of the plate. Fig. 18(d) compares the crack paths predicted in this paper with those obtained by the FEM simulations in [43] and [44] and the SBFEM simulations in [32]. These features are captured by these methods and are in good correspondence with each other. Due to the remeshing procedure, a small crack increment length can be used directly to guarantee the accuracy of the crack path with fewer polygon elements which improves the computational efficiency.

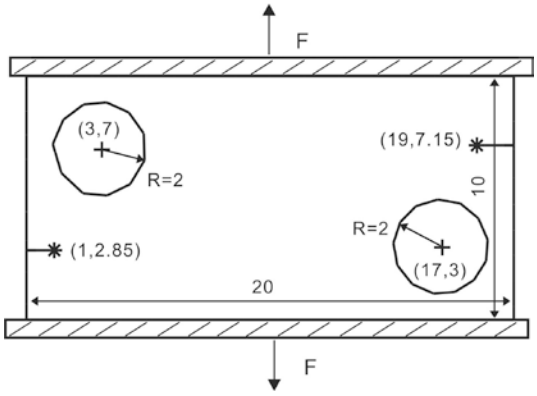

(a) Geometry(all dimensions in mm)

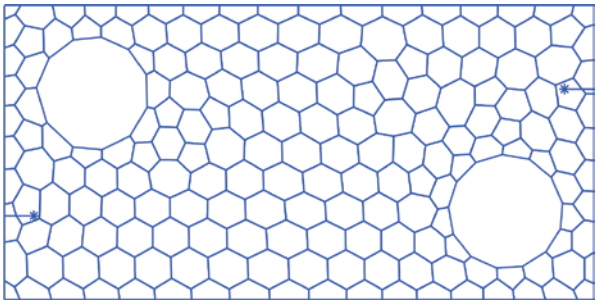

(b) The polygon SBFEM mesh

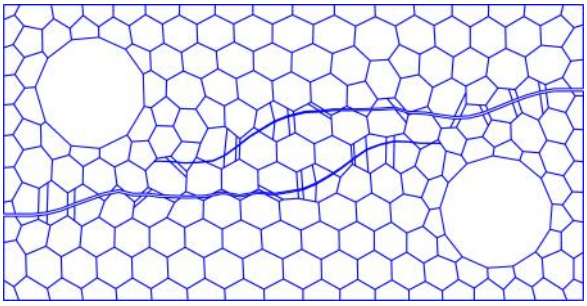

(c) Predicted final crack path

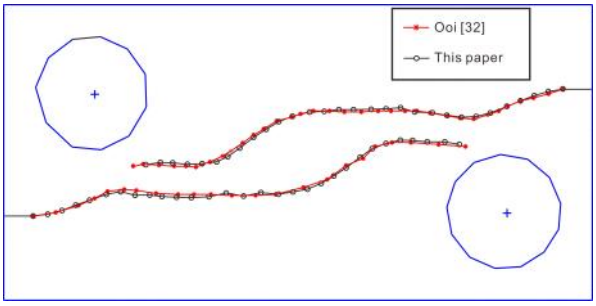

(d) Comparison of crack paths

Fig. 19 Predicted final crack paths of the plate with two holes

The final, and most challenging,example presented in this paper involves multiple crack propagation in a plate with two edge cracks and two circular holes. The geometry and material properties of the plate are shown in Fig. 19 (a). This plate is subjected to a uniform tensile stress as shown in the figure. The polygon mesh shown in Fig. 19 (b) and the crack increment length $\Delta a = 0.5mm$ are used to model the crack propagation. Compared with the coarse mesh in [32], only 189 polygon elements are contained in the polygon mesh.

The predicted crack paths of this example are shown in Fig. 19 (c). The two crack paths can be thought as symmetric due to the loading and geometry. At the beginning, each crack propagates towards the nearest hole. Then, the cracks reorient themselves almost horizontally and grow towards each other until to the middle of the plate. At the end, both cracks are attracted again by the opposite holes. Fig. 19 (d) compares the crack paths predicted in this paper with the results obtained in [32]. All these features are captured and are similar with each other.

6. Conclusion

A methodology to automatically model crack propagation in brittle materials using polygon elements has been developed in this study. The polygon element mesh is generated from an open-source Delaunay tessellation. Each polygon element is treated as a subdomain. Standard SBFEM

procedures are then used to obtain the displacements, stresses in each polygon and accurate SIFs in the cracked domain.

Compared with the previous SBFEM methodologies [28-29], the simple remeshing procedure, capable of handling problems involving complex geometries with any arbitrary polygon, is further developed to accommodate crack propagation. Based on the algorithm, minimal changes to the global mesh are made during each propagating step. The polygon optimisation implemented in this paper can guarantee accurate and stable modelling of crack propagation.

Compared with the previous polygon SBFEM methodologies [32-35] developed for crack propagation, the method developed in the paper needs fewer polygon elements to predict the crack path with a flexible crack increment length. There is also no need to store and update the triangle mesh as the background mesh.

The crack propagation paths that are predicted by the procedure agree well with other numerical results (FEM and SBFEM) in the literature. Although the current study only models static problems, further improvements on the remeshing procedure will enable dynamic problems to be simulated.

Acknowledgements:

The authors gratefully acknowledge support for this research from the National Natural Science F oundation of China (Grant Nos. 11372098 and 11132003). The first author is grateful to China Scholarship Council (CSC) for providing him a one-year scholarship to study at Durham University.

References:

[1] Ngo D, Scordelis AC. Finite element analysis of reinforced concrete beams. ACI Journal Proceedings, 1967.

[2] Prasad MVKV, Krishnamoorthy CS. Computational model for discrete crack growth in plain and reinforced concrete. Computer Methods in Applied Mechanics and Engineering. 2002;191:2699-725.

[3] Xie M, Gerstle WH. Energy-based cohesive crack propagation modeling. Journal of Engineering Mechanics. 1995;121:1349-58.

[4] Yang ZJ, Chen JF. Fully automatic modelling of cohesive discrete crack propagation in concrete beams using local arc-length methods. International Journal of Solids and Structures. 2004;41:801-26.

[5] Freitas JAT, Ji ZY. Hybrid-trefftz finite element formulation for simulation of singular stress fields. International Journal for Numerical Methods in Engineering. 1996;39:281-308.

[6] Karihaloo BL, Xiao QZ. Accurate determination of the coefficients of elastic crack tip asymptotic field by a hybrid crack element with p-adaptivity. Engineering Fracture Mechanics. 2001;68:1609-30.

[7] Bouchard PO, Bay F, Chastel Y. Numerical modelling of crack propagation: automatic remeshing

and comparison of different criteria. Computer Methods in Applied Mechanics and Engineering. 2003;192:3887-908.

[8] Khoei AR, Azadi H, Moslemi H. Modeling of crack propagation via an automatic adaptive mesh refinement based on modified superconvergent patch recovery technique. Engineering Fracture Mechanics. 2008;75:2921-45.

[9] Yagawa G, Aizawa T, Ando Y. Crack analysis of power hardening materials using a penalty function and superposition method. Proceedings of the 12th Conference on Fracture Mechanics, ASTM STP. 1980;700:439-52.

[10] Saouma VE, Schwemmer D. Numerical evaluation of the quarter-point crack tip element. International Journal for Numerical Methods in Engineering. 1984;20:1629-41.

[11] Xiao QZ, Karihaloo BL, Liu XY. Direct determination of SIF and higher order terms of mixed mode cracks by a hybrid crack element. International Journal of Fracture. 2004;125:207-25.

[12] Sukumar N, Moës N, Moran B, Belytschko T. Extended finite element method for three-dimensional crack modelling. International Journal for Numerical Methods in Engineering. 2000;48:1549-70.

[13] Zi G, Rabczuk T, Wall W. Extended meshfree methods without branch enrichment for cohesive cracks. Computational Mechanics. 2007;40:367-82.

[14] Richardson CL, Hegemann J, Sifakis E, Hellrung J, Teran JM. An XFEM method for modeling geometrically elaborate crack propagation in brittle materials. International Journal for Numerical Methods in Engineering. 2011;88:1042-65.

[15] Liu ZL, Menouillard T, Belytschko T. An XFEM/Spectral element method for dynamic crack propagation. International Journal of Fracture. 2011;169:183-98.

[16] Bordas S, Rabczuk T, Zi G. Three-dimensional crack initiation, propagation, branching and junction in non-linear materials by an extended meshfree method without asymptotic enrichment. Engineering Fracture Mechanics. 2008;75:943-60.

[17] Rabczuk T, Zi G, Bordas S, Nguyen-Xuan H. A geometrically non-linear three-dimensional cohesive crack method for reinforced concrete structures. Engineering Fracture Mechanics. 2008;75:4740-58.

[18] Ooi ET, Yang Z. Modelling dynamic crack propagation using the scaled boundary finite element method. International Journal for Numerical Methods in Engineering. 2011;88:329-49.

[19] Portela A, Aliabadi MH, Rooke DP. Dual boundary element incremental analysis of crack propagation. Computers & Structures. 1993;46:237-47.

[20] Fedelinski P. Computer modelling of dynamic fracture experiments. Key Engineering Materials. 2011;454:113-25.

[21] Simpson R, Trevelyan J. A partition of unity enriched dual boundary element method for accurate computations in fracture mechanics. Computer Methods in Applied Mechanics and Engineering. 2011;200:1-10.

[22] Wolf JP, Song CM. Finite-element modelling of unbounded media: Wiley Chichester; 1996.

[23] Song CM, Wolf JP. Semi-analytical representation of stress singularities as occurring in cracks in anisotropic multi-materials with the scaled boundary finite-element method. Computers & Structures. 2002;80:183-97.

[24] Chidgzey SR, Deeks AJ. Determination of coefficients of crack tip asymptotic fields using the scaled boundary finite element method. Engineering Fracture Mechanics. 2005;72:2019-36.

[25] Chidgzey SR, Trevelyan J, Deeks AJ. Coupling of the boundary element method and the scaled boundary finite element method for computations in fracture mechanics. Computers & Structures, 2008;86(11):1198-1203.

[26] Natarajan S, Song CM. Representation of singular fields without asymptotic enrichment in the extended finite element method. International Journal for Numerical Methods in Engineering, 2013;96(13):813-41.

[27] Natarajan S, Song CM, Belouettar S. Numerical evaluation of stress intensity factors and T-stress for interfacial cracks and cracks terminating at the interface without asymptotic enrichment. Computer Methods in Applied Mechanics and Engineering, 2014;279: 86-112.

[28] Yang ZJ. Fully automatic modelling of mixed-mode crack propagation using scaled boundary finite element method. Engineering Fracture Mechanics. 2006;73:1711-31.

[29] Yang ZJ, Deeks AJ. Fully-automatic modelling of cohesive crack growth using a finite element–scaled boundary finite element coupled method. Engineering Fracture Mechanics. 2007;74:2547-73.

[30] Ooi ET, Yang ZJ. Modelling multiple cohesive crack propagation using a finite element–scaled boundary finite element coupled method. Engineering Analysis with Boundary Elements. 2009;33:915-29.

[31] Ooi ET, Yang ZJ. Efficient prediction of deterministic size effects using the scaled boundary finite element method. Engineering Fracture Mechanics. 2010;77:985-1000.

[32] Ooi ET, Song CM, Tin-Loi F, Yang ZJ. Polygon scaled boundary finite elements for crack propagation modelling. International Journal for Numerical Methods in Engineering. 2012;91:319-42.

[33] Ooi ET, Song CM, Tin-Loi F, Yang ZJ. Automatic modelling of cohesive crack propagation in concrete using polygon scaled boundary finite elements. Engineering Fracture Mechanics. 2012;93:13-33.

[34] Ooi ET, Shi M, Song CM, Tin-Loi F, Yang Z. Dynamic crack propagation simulation with scaled boundary polygon elements and automatic remeshing technique. Engineering Fracture Mechanics. 2013;106:1-21.

[35] Shi MG, Zhong H, Ooi ET, Zhang C, Song CM. Modelling of crack propagation of gravity dams by scaled boundary polygons and cohesive crack model. International Journal of Fracture. 2013;183:29-48.

[36] Ooi ET, Yang ZJ. A hybrid finite element-scaled boundary finite element method for crack propagation modelling. Computer Methods in Applied Mechanics and Engineering. 2010;199:1178-92.

[37] Ooi ET, Yang ZJ. Modelling crack propagation in reinforced concrete using a hybrid finite element-scaled boundary finite element method. Engineering Fracture Mechanics. 2011;78:252-73.

[38] Natarajan S, Ooi ET, Chiong I, Song CM. Convergence and accuracy of displacement based finite element formulations over arbitrary polygons: Laplace interpolants, strain smoothing and scaled boundary polygon formulation. Finite Elements in Analysis and Design, 2014;85: 101-22.

[39] Ooi E T, Song CM, Tin-Loi F. A scaled boundary polygon formulation for elasto-plastic analyses. Computer Methods in Applied Mechanics and Engineering, 2014;268:905-37.

[40] Deeks AJ, Wolf JP. A virtual work derivation of the scaled boundary finite-element method for elastostatics. Computational Mechanics. 2002;28:489-504.

[41] Anon. DistMesh - A Simple Mesh Generator in MATLAB. (online) Available at: http://people.sc.fsu.edu/~jburkardt/m_src/distmesh/distmesh.html .

[42] Swenson DV, Kaushik N. Finite element analysis of edge cracking in plates. Engineering Fracture Mechanics. 1990;37:641-52.

[43] Rashid MM. The arbitrary local mesh replacement method: an alternative to remeshing for crack propagation analysis. Computer Methods in Applied Mechanics and Engineering. 1998;154:133-50.

[44] Bouchard PO, Bay F, Chastel Y, Tovena I. Crack propagation modelling using an advanced remeshing technique. Computer Methods in Applied Mechanics and Engineering. 2000;189:723-42.